ELECTRONIC SUPPLEMENTARY INFORMATION

Interplay between Ligand Mobility and Nanoparticle Geometry during Cellular Uptake of PEGylated Liposome and Bicelle

Zhiqiang Shen
Department of Mechanical Engineering, University of Connecticut, Storrs, CT 06269, USA

Huilin Ye
Department of Mechanical Engineering, University of Connecticut, Storrs, CT 06269, USA

Martin Kröger
Department of Materials, Polymer Physics, ETH Zurich, CH-8093 Zurich, Switzerland

Shan Tang
State Key Laboratory of Structural Analysis for Industrial Equipment, Department of Engineering Mechanics, and International Research Center for Computational Mechanics, Dalian University of Technology, Dalian, 116023, PR China
E-mail: shantang@dlut.edu.cn

Ying Li
Department of Mechanical Engineering and Institute of Materials Science, University of Connecticut, Storrs, CT 06269, USA
E-mail: yingli@engr.uconn.edu

Contents

1. Computational Model and Methodology

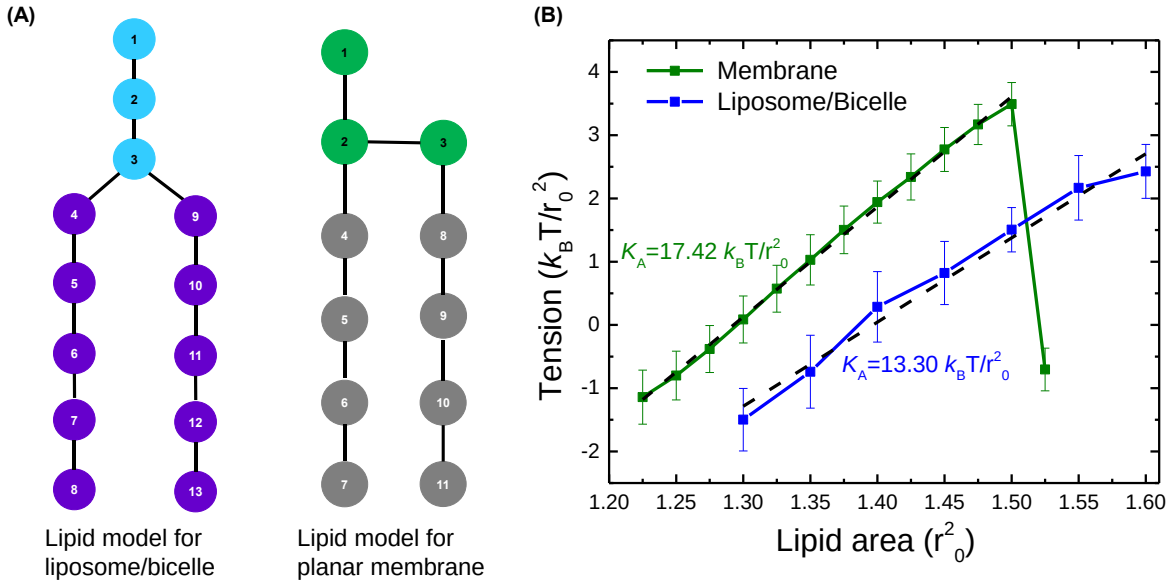

Figure S1: (A) Lipid models for liposome/bicelle (beads 1–13) and planar membrane (beads 1–11). (B) Relation between membrane tension and lipid area for the (blue) lipids model of the liposome/bicelle and (green) lipid model of the planar membrane.

1.1. Lipid Model

The lipid models for liposome/bicelle and planar membrane are given in Fig. S1(A). In the liposome/bicelle model, the head group of lipid molecule is represented by three linearly

connected hydrophilic beads, while each of the two tails is represented by 5 hydrophobic beads. Neighboring beads i and j are connected by harmonic spring potentials,

$$U_{s1} = K_{s1}(r_{ij} - r_{s1})^2, \tag{1}$$

where the spring constant $K_{s1} = 50\ k_{\rm B}T/r_0^2$ and the equilibrium bond length $r_{s1} = 0.7\ r_0$ [1]. The stiffness of head and tail groups is controlled by an bending potential applied on the adjacent three beads,

$$U_{\vartheta 1} = K_{\vartheta 1}(\vartheta - \vartheta_0)^2, \tag{2}$$

where $K_{\vartheta 1}$, ϑ and ϑ_0 are the bending constant, the inclination angle and the equilibrium angle, respectively. Different $K_{\vartheta 1}$ and ϑ_0 values are used to reflect the flexibility in different locations of each lipid molecule [1]. For three consecutive lipid head/tail beads in the lipid, $K_{\vartheta 1} = 3.0\ k_{\rm B}T$ and $\vartheta_0 = 180^\circ$. For beads 3, 4, and 9, $K_{\vartheta 1} = 1.5\ k_{\rm B}T$ and $\vartheta_0 = 120^\circ$. For the two consecutive head beads connected to the first bead in the tail (beads 2, 3, 4 and beads 2, 3, 9), $K_{\vartheta 1} = 2.25\ k_{\rm B}T$ and $\vartheta_0 = 120^\circ$. Due the flexible head group in this DPPC lipid model, the energy penalty to form the bilayer edge in the bicelle is relatively small, facilitating the formation of a larger sized bicelle.

In the model for the planar membrane, adjacent beads making the lipid molecules are connected by harmonic springs,

$$U_{s2} = K_{s2}(r_{ij} - r_{s2})^2, \tag{3}$$

with spring coefficient $K_{s2} = 64\ k_{\rm B}T/r_0^2$ and equilibrium distance $r_{s2} = 0.5r_0$ [2, 3]. The stiffness of the lipid tails is guaranteed by a bending potential

$$U_{\vartheta 2} = K_{\vartheta 2}(1 - \cos\vartheta), \tag{4}$$

where $K_{\vartheta 2} = 15k_{\rm B}T$ [2, 3].

All pair-wise interactions parameters a_{ij} between lipid beads are listed in Table S1. Note that a larger repulsion between lipids in the liposome/bicelle and membrane is used to avoid their possible fusion. Under control of these parameters, the bilayer thickness in the liposome/bicelle is around $d_{\rm HH1} = 5r_0$. The bilayer thickness in the planar membrane is around $d_{\rm HH2} = 4r_0$. The mechanical properties of these two lipid models are calibrated through stretching a patch of a planar bilayer in the simulation box of size $(50 \times 50 \times 50)\ r_0^3$. The relations between the tension of the planar bilayer and the lipid molecular area for these two lipid models are given in Fig. S1(B). The stretch modulus can be extracted from the slope of these curves. For the lipid bilayer in the liposome/bicelle, its stretch modulus is $K_{A1} = 13.30\ k_{\rm B}T/r_0^2$, while the one for the planar membrane is $K_{A2} = 17.42\ k_{\rm B}T/r_0^2$. The corresponding bending rigidity can be obtained from $\kappa = K_A d_{\rm HH}^2/48$ [4, 5]. The bending rigidity of the liposome/bicelle is therefore $\kappa_{\rm lip} \approx 7k_{\rm B}T$; the bending rigidity of membrane is $\kappa_{\rm m} \approx 6k_{\rm B}T$. Additionally, to estimate the line tension of the bilayer for liposome/bicelle, we systematically change the size of the bicelle to find the transition size from bicelle to liposome $R_{\rm trans} \approx 10r_0$. The line tension of the bicelle can be estimated via $\lambda = 2\kappa_{\rm lip}/R_{\rm trans}$ [6], resulting in $\lambda \approx 1.4k_{\rm B}T/r_0$. Note that the transition size increases when the lipid heads get decorated with PEG polymers.

Table S1: Interaction parameters, a_{ij} in units of $k_{\mathrm{B}}T$, between lipid bead types i and j, in the DPD simulation. S and E represent solvent (water) and PEG beads, respectively. H_1 and T_1 represent the lipid head and tail beads for liposome/bicelle. H_2 and T_2 represent the lipid head and tail beads for the planar membrane.

	S	H_2	T_2	H_1	T_1	E
S	25.0	30.0	75.0	25.0	100.0	26.3
H_2	30.0	30.0	35.0	100.0	100.0	26.3
T_2	75.0	35.0	10.0	100.0	100.0	33.7
H_1	25.0	100.0	100.0	25.0	100.0	26.3
T_1	100.0	100.0	100.0	100.0	25.0	33.7
E	26.3	26.3	33.7	26.3	33.7	25.0

1.2. PEG model

A hydrophilic PEG polymer in our DPD simulations is modeled by a linear chain consisting of coarse-grained monomers. The PEG monomers are linearly connected by the harmonic bond potential $U_{s3} = K_{s3}(r_{ij} - r_{s3})^2$, with spring stiffness $K_{s3} = 2111.3\, k_{\mathrm{B}}T/r_0^2$ and equilibrium distance $r_{s3} = 0.4125\, r_0$. The semi-flexibility of the PEG polymer is taken into account by adding the bending potential $U_{\vartheta 3} = K_{\vartheta 3}(\cos\vartheta - \cos\vartheta_{03})^2$, with bending stiffness $K_{\theta 3} = 16.4946\, k_{\mathrm{B}}T$, and equilibrium bending angle $\theta_{03} = 130\,^\circ$ between each three consecutive monomers. Such a DPD PEG model could correctly reproduce the conformation of a PEG polymer in water, including the radius of gyration and end-to-end distance, as shown in our previous studies. [7, 8] To describe the PEGylated lipid, one end of the PEG polymer is bonded to the lipid head bead through a harmonic bond potential. In addition, the monomers at the free end of PEG polymers are defined to act as targeting moieties (ligands). The polymerization degree of PEG polymers in our simulation is set as $N = 20$ (representing a molecular weight around 660 Da), falling within the typical range of 500-3000 Da in experiments. [9–11]

Within our DPD model, different types of beads have identical masses and cutoff distances for pairwise interactions. For the sake of transferability, the mass, length and time scales are all normalized. The unit length is taken to be the cutoff distance r_0. The unit mass is m for all the beads and is set to unity. In addition, the unit energy is defined by the thermal energy $k_{\mathrm{B}}T$. All other dimensional quantities can thus be uniquely made dimensionless in terms of these basic units (and vice versa). The time step in our DPD simulations is chosen as $\Delta t = 0.01\tau$, with $\tau = \sqrt{mr_0^2/k_{\mathrm{B}}T}$. The number density of beads in the simulation box is fixed at $3/r_0^3$ [12]. The velocity-Verlet integration algorithm is adopted for the time integration. The reduced units can be mapped to SI units using a real bilayer thickness and a measured value for the in-plane diffusion coefficient of lipids, as shown in previous studies [2, 3]. From the experiments, the thickness of the membrane is $d_{\mathrm{HH}} \approx 3.53$ nm [13] and the thickness of the planar membrane in our simulation is $d_{\mathrm{HH}} \approx 4$

r_0. The physical length scale could then be obtained as $r_0 \simeq 0.9$ nm. Comparing the experimental lipid lateral diffusion coefficient $D \simeq 5$ μm^2/s of the DMPC [14] with the one from our simulation $D \simeq 7.3 \times 10^{-2}\, r_0^2/\tau$, we obtain the physical time scale $\tau = 11.8$ ns. Periodic boundary conditions are applied along all directions of the simulation box. All the simulations are performed by using the Large-scale Atomic/Molecular Massively Parallel Simulator (LAMMPS), distributed by Sandia National Laboratories [15].

1.3. N-varid method

Due to the elasticity of the lipid membrane, the tension of membranes in cells can be adjusted, changing from 0.01 to 10 mN/m. [16] The N-varied DPD method is applied during the membrane wrapping process to ensure a constant tension of the planar membrane. [7,8,17–19] In practice, boundaries of the lipid bilayer are treated as a lipid reservoir for addition and removal of lipids. If the lipid number per unit area is larger (or smaller) than the target density ρ, lipid molecules will be deleted (or inserted) into this boundary region to maintain a constant lipid number density. Meanwhile, a corresponding number of water molecules will be randomly inserted into (or deleted from) the simulation box to ensure a constant bead density of $3.0/r_0^3$ in the simulation box. The target density ρ is taken based on the relation between membrane tension and lipid area given in Fig. S1. By using the N-varied DPD protocol, the lipid density in the membrane can easily be controlled to maintain the membrane's lateral tension during the membrane wrapping process.

1.4. Simulation Protocol

To prepare a PEGylated liposome, lipid molecules are firstly randomly placed into a simulation box to form a liposome through a self-assembly process at temperature $T = 1.0$. Subsequently, a certain number of lipids in the outer layer is randomly chosen to be grafted with PEG chains on the lipid head beads, in accord with the molar ratio of the targeted PEGylated lipid. A PEGylated liposome then further relaxes for a duration of $10^6\,\tau$ at $T = 1.0$. To prepare a PEGylated bicelle, a small patch of a planar bilayer is first relaxed in a simulation box. Afterwards, as certain number of lipids in the upper and lower leaflet are randomly chosen to graft with PEG chains on the lipid head beads. Afterwards, we enlarge the simulation box in the lateral direction while keeping the size of the PEGylated bilayer. The space in the edge of simulation box is filled with water to the keep the density of the system unaltered. A PEGylated bicelle is obtained by relaxing the system for $10^6\,\tau$ at $T = 1.0$. The planar membrane bilayer is relaxed in the box of size $(70 \times 70 \times 100)\, r_0^3$, which is large enough to avoid an influence of simulation box size on endocytosis. Finally, the fully relaxed PEGylated liposomes are placed above the planar bilayer to investigate the membrane wrapping process.

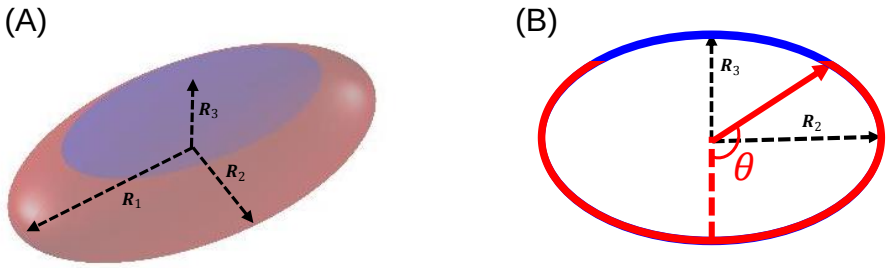

Figure S2: (A) Illustration of membrane wrapping for an ellipsoidal NPs. The three principle radii of the ellipsoid are R_1, R_2 and R_3. The red part in the NP denotes the region that wrapped by membrane. While the blue part of the NP represents the unwrapped part of NP. (B) Illustration of cross cutting of the ellipsoidal NP.

1.5. Computation of membrane energy

To estimate the membrane elastic energy, we assume that a planar membrane wraps around a ellipsoidal NPs as given in Fig. S2(A). The three principle radii of the ellipsoid we denote by R_1, R_2 and R_3. The ellipsoidal surface can be parameterized as

$$x = R_1 \cos\phi \sin\theta, \quad y = R_2 \sin\phi \sin\theta, \quad z = R_3 \cos\theta, \tag{5}$$

where $0 \leq \theta < \pi$ and $0 \leq \phi < 2\pi$. When $R_1 = R_2 = R_3$, the ellipsoid returns to a spherical shape. If $R_1 = R_2$, the ellipsoid is symmetric in the plane of the membrane. An area element dS and the mean curvature H on any point of the ellipsoidal surface can be expressed as the function of θ and ϕ as follows [20]

$$dS(\theta,\phi) = \sin(\theta)\sqrt{R_c^2 \sin^2\theta(R_1^2 \sin^2\phi + R_2^2 \cos^2\phi) + R_1^2 R_2^2 \cos^2\theta}\, d\phi d\theta, \tag{6}$$

$$H(\theta,\phi) = \frac{R_1 R_2 R_3[3(R_1^2+R_2^2)+2R_3^2+(R_1^2+R_2^2-2R_3^2)\cos(2\theta)-2(R_1^2-R_2^2)\cos(2\phi)\sin^2\theta]}{8\{R_1^2 R_2^2 \cos^2\theta + R_3^2[R_2^2\cos^2\phi + R_1^2\sin^2\phi]\sin^2\theta\}^{3/2}} \tag{7}$$

For simplicity, we consider a membrane patch that wraps around the NPs. Additionally, we assume that the membrane wrapping follows the evolution of θ as given in Fig. S2(B). Therefore, the wrapping fraction f of the ellipsoidal NPs is a function of parameter θ only, and defined by

$$f(\theta) = \frac{\int_0^\theta \int_0^{2\pi} dS(\theta',\phi)}{\int_0^\pi \int_0^{2\pi} dS(\theta',\phi)}, \tag{8}$$

with $dS(\theta',\phi)$ from Eq. 6. According to Helfrich's theory [21, 22], the membrane elastic energy can be expressed as:

$$E_{\rm m} = E_{\rm mbend} + E_{\rm mtens} = 2\kappa_{\rm m} \int H^2 dS \; + \sigma \Delta S, \tag{9}$$

where $\kappa_{\rm m}$ is the bending rigidity of the membrane, σ is the membrane tension, and ΔS is the excess area induced by membrane bending. Specifically, with the area element dS and mean

curvature H at hand, the membrane bending energy at a certain wrapping fraction f can be written as

$$E_{\mathrm{mbend}}(\theta) = 2\kappa_{\mathrm{m}} \int_0^{\theta} \int_0^{2\pi} H^2(\theta', \phi) dS(\theta', \phi). \tag{10}$$

Additionally, the membrane stretching energy can be obtained as:

$$E_{\mathrm{mtens}}(\theta) = \sigma \left[\int_0^{\theta} \int_0^{2\pi} dS(\theta', \phi) \ - \pi R_1 \sin(\theta) R_2 \sin(\theta) \right]. \tag{11}$$

As we can see for the expressions above, the membrane elastic energy is a function of θ. The integrals cannot be performed analytically; the integral over ϕ alone can be expressed in terms of an elliptic integral. Given the expressions of Eqs. 8, 10 and 11, the critical membrane tension can be directly obtained by following the Eq. 4 in the main text.

2. Results

2.1. Membrane wrapping process for PEGylated liposome under the membrane tension of $0.09k_BT/r_0^2$

The membrane wrapping processes for PEGylated liposomes with PEG molar ratios of 50% mol, 60% mol and 70% mol are given in Fig. S3. The membrane tension of these three cases is maintained at $0.09k_{\mathrm{B}}T/r_0^2$. As we can see from Fig. S3(A) at 50% mol, the PEGylated liposome quickly adheres on the membrane due to the ligand-receptor binding (at $t = 59$ μs). Additionally, the membrane starts to bend and wrap around the liposome. During this process, the PEG polymers keep aggregating within the wrapped region of the liposome. Finally, the liposome is partially wrapped and trapped on the membrane. The membrane wrapping process of 40% mol PEGylated liposome is similar to the one of the 50% mol PEGylated liposome. The membrane wrapping process of 60% mol PEGylated liposome as shown in Fig. S3(B) is however different. Along with the aggregation of PEG polymers at $t = 280$ μs, the lipids on the contact edge of the liposome start to protrude and to assume a tubular shape. This protruding of the lipid might help releasing the increased steric interaction caused by aggregation. Furthermore, with the formation of a tubular shape, the space occupied by the water inside is decreased (at $t = 1000$ μs). Finally, the 60% mol PEGylated liposome is also trapped on the membrane. At 70% mol, the lipids on the contact edge of the liposome protrude as well. Moreover, with the increase of PEG polymer number, the tubular shape further reduces the space available to water, which in turns produces a large osmotic pressure, ultimately leading to liposome rupture at $t = 210$ μs. Finally, the ruptured 70% mol PEGylated liposome deforms into a strip-like shape that is trapped on the membrane.

2.2. Membrane wrapping process for PEGylated bicelle under the membrane tension of $0.09k_BT/r_0^2$

The membrane wrapping processes for the PEGylated bicelle with PEG molar ratios of 50% and 70% mol are given in Fig. S4. The membrane tension for the two cases is maintained at $0.09k_{\mathrm{B}}T/r_0^2$. At 50% mol, the PEGylated bicelle is finally trapped on the membrane and the bicelle keeps a disc-like shape during the whole membrane wrapping process. The membrane wrapping process of the 40% mol PEGylated bicelle is similar to that of the 50% mol PEGylated bicelle. At 70% mol, the PEGylated bicelle is also partially wrapped. Interestingly, with the aggregation of PEG polymers in the wrapped region, the bicelle deforms into a strip-like shape to release the increased steric force. The membrane wrapping process of 60% mol PEGylated bicelle is similar to the that of 70% mol PEGylated bicelle at the membrane tension of $0.09k_{\mathrm{B}}T/r_0^2$.

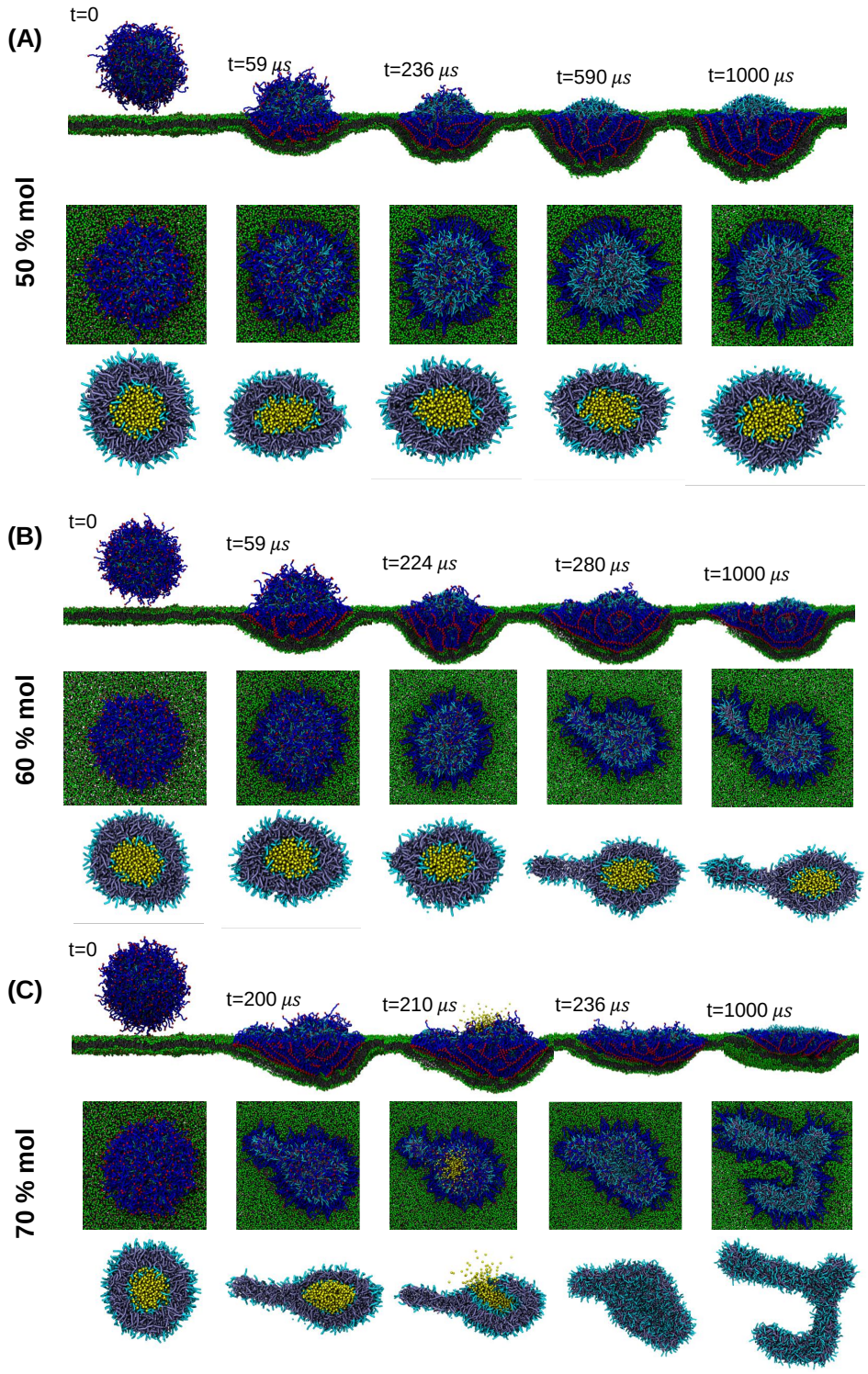

Figure S3: Membrane wrapping process for PEGylated liposome under the membrane tension of $0.09 k_{\mathrm{B}} T / r_0^2$. (A-C) Snapshots during membrane wrapping process for PEGylated liposomes with PEG molar ratios of 50 %mol, 60 %mol, and 70 %mol.

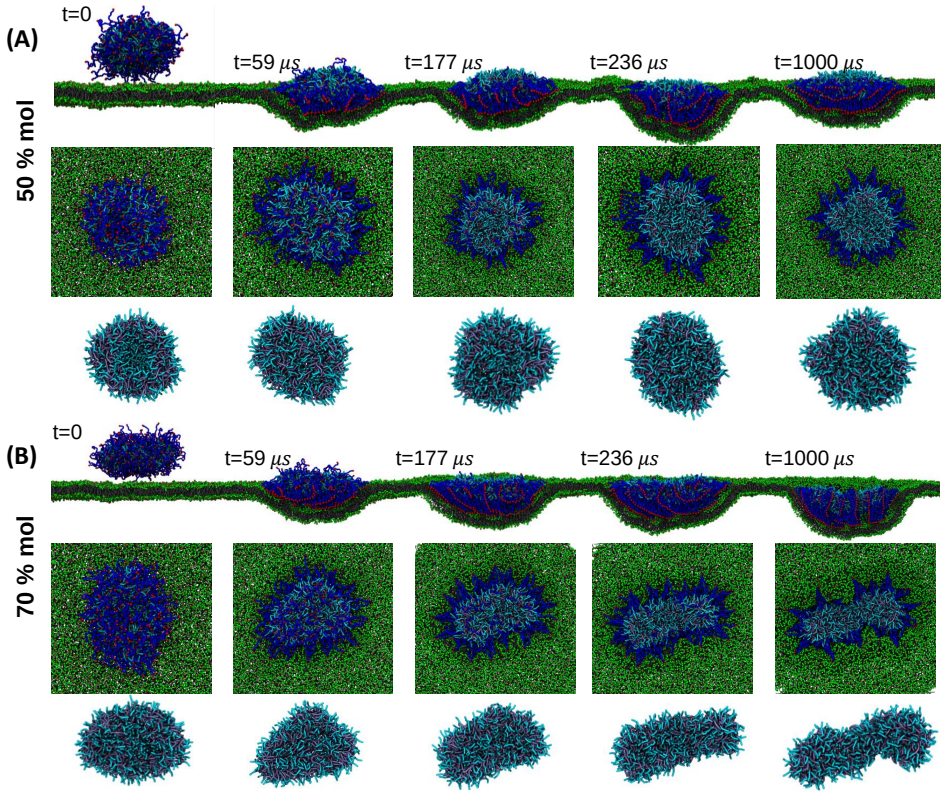

Figure S4: Membrane wrapping process for the PEGylated bicelle under membrane tension of $0.09 k_{\mathrm{B}} T / r_0^2$. (A-B) Snapshots taken during the membrane wrapping processes for PEGylated liposomes with PEG molar ratios of 50% mol and 70% mol.

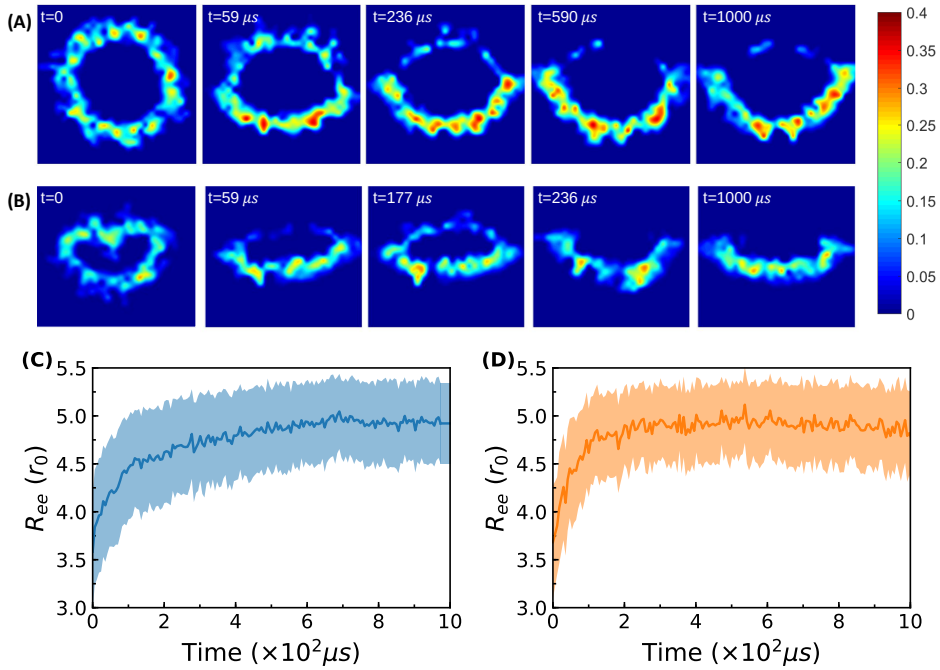

Figure S5: Projected PEG volume fraction distribution and end-to-end distance. Evolution of the PEG volume fraction distribution of the (A) PEGylated liposome and (B) PEGylated bicelle. Evolution of PEG polymers end-to-end distance for (C) PEGylated liposome and (D) PEGylated bicelle. The PEG molar ratio for both liposome and bicelle is 50% mol; the membrane tension is $0.09k_{\mathrm{B}}T/r_0^2$ for both liposome and bicelle. Because of the partially wrapped state at the end, the PEG volume fraction remains highly inhomogeneous. Also, the end-to-end distance of PEG polymers remains at a large value.

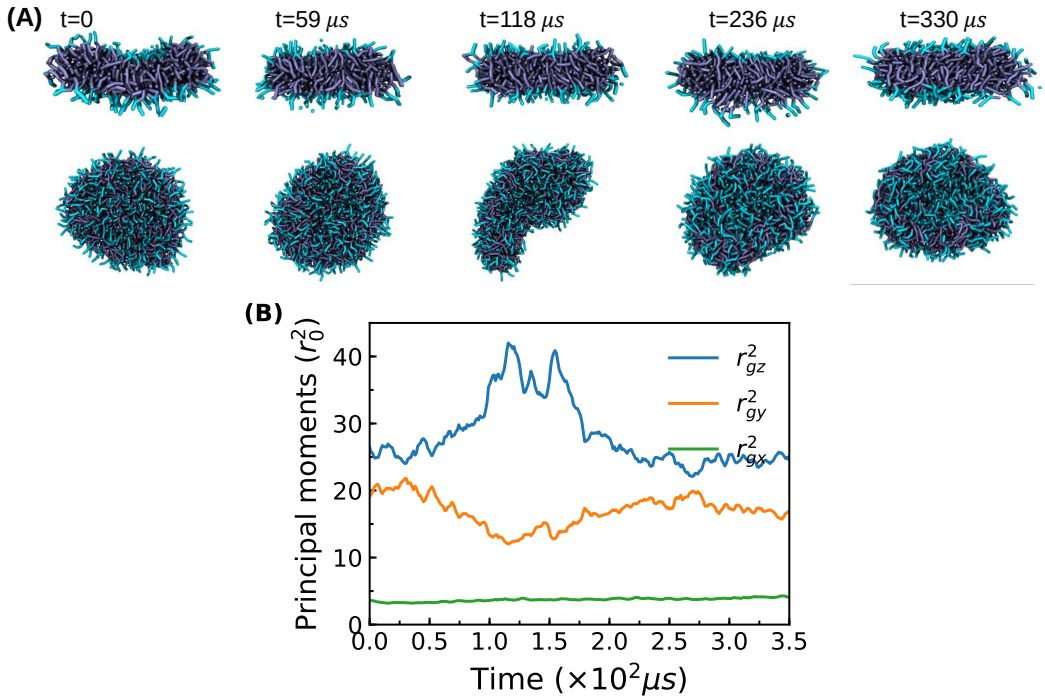

Figure S6: (A) Snapshots of bicelle deformation during the membrane wrapping process. The configurations in the upper panel are cross cuttings of the bicelle at different times. The snapshots in the lower panel are the corresponding top views of the same bicelles. (B) Evolution of the three principal moments of the gyration tensor of the bicelle during the membrane wrapping process. The corresponding snapshots of the membrane wrapping process are given in Fig. 2(B) in the main text. The snapshots of cross cuttings in (A) show a flat surface plane for the bicelle during the entire wrapping process. In (B), the in–plane principal moments r_{gz}^2 and r_{gy}^2 change dramatically during the deformation of the bicelle, while the out–of–plane plane principal moment r_{gx}^2 keeps almost constant at a small value. The cross cutting of the bicelle in (A) and the principal moment r_{gx}^2 suggest that the curvature of the bicelle barely changes during the membrane wrapping process.

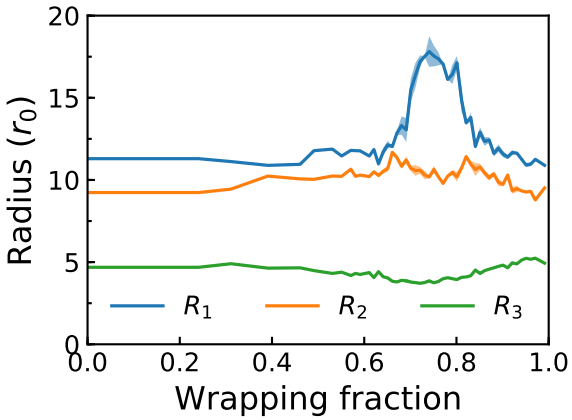

Figure S7: Evolution of the three principle radii belonging to the fitted ellipsoids of the PEGylated bicelle. The corresponding snapshots of the membrane wrapping process are given in Fig. 2(B) in the main text. Based on the data shown here, the three principle radii of the PEGylated bicelle at the most deformed state around the critical wrapping fraction f_c are $R_1 \approx 19\, r_0$, $R_2 \approx 10\, r_0$, and $R_3 \approx 4\, r_0$, respectively.

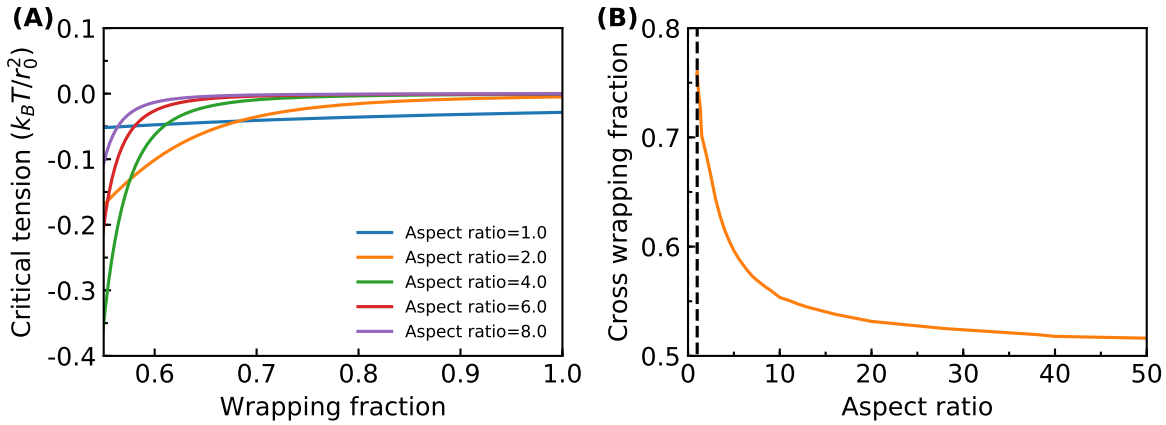

Figure S8: (A) Comparison between critical membrane tensions of spherical and oblate NPs. The surface area of these NPs is assumed to be identical. The radius of the spherical NP is taken as $R = 14.5\, r_0$. The shape of the oblate ellipsoidal NP is specified by $R_1 = R_2 > R_3$, where R_1, R_2 and R_3 are its principle radii. The curve with aspect ratio $R_1/R_3 = 1$ represents the spherical NPs. The membrane bending rigidity is taken as $6\ k_{\mathrm{B}}T$. (B) Cross wrapping fraction against aspect ratio R_1/R_3. The cross wrapping fraction is defined as the wrapping fraction where the oblate starts to have a larger critical membrane tension.

References

[1] Robert D. Groot and K. L. Rabone. Mesoscopic simulation of cell membrane damage, morphology change and rupture by nonionic surfactants. *Biophys. J.*, 81:725–736, 2001.

[2] Andrea Grafmüller, Julian Shillcock, and Reinhard Lipowsky. Pathway of membrane fusion with two tension-dependent energy barriers. *Phys. Rev. Lett.*, 98:218101, 2007.

[3] Andrea Grafmüller, Julian Shillcock, and Reinhard Lipowsky. The fusion of membranes and vesicles: pathway and energy barriers from dissipative particle dynamics. *Biophys. J.*, 96:2658–2675, 2009.

[4] M. Mutz and W. Helfrich. Bending rigidities of some biological model membranes as obtained from the fourier analysis of contour sections. *J. Phys.*, 51:991–1001, 1990.

[5] Rüdiger Goetz, Gerhard Gompper, and Reinhard Lipowsky. Mobility and elasticity of self-assembled membranes. *Phys. Rev. Lett.*, 82:221, 1999.

[6] Changjin Huang, David Quinn, Yoel Sadovsky, Subra Suresh, and K Jimmy Hsia. Formation and size distribution of self-assembled vesicles. *Proc. Natl. Acad. Sci. U.S.A.*, 114:1910–2915, 2017.

[7] Ying Li, Martin Kröger, and Wing Kam Liu. Endocytosis of pegylated nanoparticles accompanied by structural and free energy changes of the grafted polyethylene glycol. *Biomaterials*, 35:8467–8478, 2014.

[8] Ying Li, Martin Kröger, and Wing Kam Liu. Shape effect in cellular uptake of pegylated nanoparticles: comparison between sphere, rod, cube and disk. *Nanoscale*, 7:16631–16646, 2015.

[9] Eun Chul Cho, Leslie Au, Qiang Zhang, and Younan Xia. The effects of size, shape, and surface functional group of gold nanostructures on their adsorption and internalization by cells. *Small*, 6(4):517–522, 2010.

[10] Carl D Walkey, Jonathan B Olsen, Hongbo Guo, Andrew Emili, and Warren C. W. Chan. Nanoparticle size and surface chemistry determine serum protein adsorption and macrophage uptake. *J. Am. Chem. Soc.*, 134(4):2139–2147, 2012.

[11] Adam de la Zerda, Sunil Bodapati, Robert Teed, Salomon Y May, Scott M Tabakman, Zhuang Liu, Butrus T Khuri-Yakub, Xiaoyuan Chen, Hongjie Dai, and Sanjiv S Gambhir. Family of enhanced photoacoustic imaging agents for high-sensitivity and multiplexing studies in living mice. *ACS Nano*, 6(6):4694–4701, 2012.

[12] Robert D. Groot and Patrick B. Warren. Dissipative particle dynamics: Bridging the gap between atomistic and mesoscopic simulation. *J. Chem. Phys.*, 107:4423, 1997.

[13] Norbert Kučerka, Yufeng Liu, Nanjun Chu, Horia I Petrache, Stephanie Tristram-Nagle, and John F Nagle. Structure of fully hydrated fluid phase dmpc and dlpc lipid bilayers using x-ray scattering from oriented multilamellar arrays and from unilamellar vesicles. *Biophys. J.*, 88:2626–2637, 2005.

[14] Greger Orädd, Göran Lindblom, and Philip W Westerman. Lateral diffusion of cholesterol and dimyristoylphosphatidylcholine in a lipid bilayer measured by pulsed field gradient nmr spectroscopy. *Biophys. J.*, 83:2702–2704, 2002.

[15] Steve Plimpton. Fast parallel algorithms for short-range molecular dynamics. *J. Comput. Phys.*, 117:1–19, 1995.

[16] Nils C Gauthier, Thomas A Masters, and Michael P Sheetz. Mechanical feedback between membrane tension and dynamics. *Trends Cell Biol.*, 22(10):527–535, 2012.

[17] Bingbing Hong, Feng Qiu, Hongdong Zhang, and Yuliang Yang. Budding dynamics of individual domains in multicomponent membranes simulated by n-varied dissipative particle dynamics. *J. Phys. Chem. B*, 111(21):5837–5849, 2007.

[18] Hong-Ming Ding and Yu-Qiang Ma. Computer simulation of the role of protein corona in cellular delivery of nanoparticles. *Biomaterials*, 35(30):8703–8710, 2014.

[19] Ye Li, Xianren Zhang, and Dapeng Cao. Nanoparticle hardness controls the internalization pathway for drug delivery. *Nanoscale*, 7(6):2758–2769, 2015.

[20] John W Harris and Horst Stöcker. *Handbook of Mathematics and Computational Science*. Springer Science & Business Media, 1998.

[21] Wolfgang Helfrich. Elastic properties of lipid bilayers: theory and possible experiments. *Z. Naturforsch. C*, 28:693–703, 1973.

[22] Frank Jülicher and Reinhard Lipowsky. Domain-induced budding of vesicles. *Phys. Rev. Lett.*, 70:2964, 1993.